doi:10.1038/nature12021

Sulphur Isotope Database:

An extensive sulphur isotope database was used in the construction of Main Text Figure 1. These data were compiled from primary references[1-37], although in some cases age constraints for certain units were obtained from other sources[38-41] or estimated. For Main Text Figure 1b, we calculated the cumulative average $\Delta^{33}S$ value for all samples up to each year of publication. The average values reported here thus include some contribution from sulphate minerals. However, the overwhelming majority of the data are sulphide mineral phases, and given that most sulphate data are characterized by negative $\Delta^{33}S$ values their inclusion will largely attenuate the pattern emphasized here, rendering our argument conservative. Furthermore, the overall effect of their inclusion is quite small (Fig. S1a,b). We also examined the effect of filtering data from analyses made via secondary ion mass spectrometry (SIMS) and analyses of macroscopic pyrite textures, which are not likely to be representative of bulk weathering crust, but again note that the basic pattern remains unchanged (Fig. S1a,b).

The mean $\Delta^{33}S$ values shown in Fig. 1 are presented as unweighted averages. We consider this approach qualitatively justified, in that the database is composed largely of fine-grained siliciclastic sedimentary rocks that are relatively organic carbon and sulphur rich. Such rocks will not only be, on average, the most sulphur-enriched phases of the crust, but they will also likely hold the majority of the weathering sulphur reservoir at Earth's surface. Nonetheless, it is important to consider the possibility that there is a bias related to systematic relationships between the sulphur content of sedimentary rocks and their $\Delta^{33}S$ value. For this purpose, we compiled the available sulphur concentration data for the units within the isotope database and performed concentration-weighted statistical analyses.

There does not appear to be any systematic relationship between rare sulphur isotope composition and sulphur content within the database (Fig. S2a). In addition, the cumulative unweighted average is nearly indistinguishable from the concentration-weighted average within this subset of the database (Fig. S2a,b). When the evolution of the overall $\Delta^{33}S$ value of the database is concentration-weighted, it shows a generally similar pattern through time to that of the overall mean values (Fig. S2b). Indeed, the mean $\Delta^{33}S$ value when weighted by concentration is more positive than the unweighted mean for a given population from the database. We stress the caveat that many of the published rare sulphur isotope datasets do not contain sulphur concentration data, so unfortunately this analysis cannot be performed on the entire database. However, the coupled isotope and concentration data represent well over 500 samples that range in sulphur content over three orders of magnitude. These considerations lead us to conclude that the pattern expressed in the overall mean $\Delta^{33}S$ values through time is robust and is not subject to a concentration bias.

The ultimate origin of the observed asymmetry in the $\Delta^{33}S$ record (i.e., the presence of a weatherable sulphur reservoir with a positive $\Delta^{33}S$ value) can be linked to the relative transport and removal processes of the two main sulphur redox species upon introduction to the hydrosphere – sulphate aerosols, which transfer negative $\Delta^{33}S$ anomalies, and zero-valent sulphur, which carries positive $\Delta^{33}S$ anomalies. Atmospheric sulphate aerosols would have been

incorporated into the relatively well-mixed seawater sulphate reservoir and a significant portion of this reservoir would thus have been sequestered in deep-sea sediments through hydrothermal[42-44] (thermochemical) or microbial sulphate reduction and subsequently subducted into an isotopically well-buffered mantle. In contrast to atmospherically derived sulphate, elemental sulphur aerosols would be much less likely to become incorporated into sedimentary sulphides forming in deep-sea environments. Elemental sulphur aerosols would typically have much more limited transport from point sources associated with subaerial volcanism[45,46], a result of limited aqueous solubility of elemental sulphur in systems that are not sulphide-buffered[47]. The end result of these processes would have been preferential burial of sulphur with positive $\Delta^{33}S$ values in marginal and epicontinental settings, which will have a higher potential (than deep-sea sediments) of becoming incorporated into the weatherable shell. In other words, the empirical record is asymmetric, and this is exactly what one would predict considering the current paradigm for the formation and transport of $\Delta^{33}S$ anomalies.

To roughly illustrate this in a quantitative way, we can envision a mass balance for Earth surface sulphur:

$$\frac{\mathrm{d}M_{surface}}{\mathrm{d}t} = F_{in} - F_C - F_S \ , \tag{1}$$

where F_{in} is the input flux to the surface, F_C represents sulphur buried into the crust (and which will later be weathered at the surface), and F_S represents sulphur lost to subduction. Isotope mass balance is given by:

$$\frac{\mathrm{d}}{\mathrm{d}t}\left(\Delta^{33}_{surface} M_{surface}\right) = \Delta^{33}_{in} F_{in} - \Delta^{33}_{C} F_C - \Delta^{33}_{S} F_S \ , \tag{2}$$

where Δ^{33}_{i} represents the deviation from mass-dependent fractionation with respect to a given flux i. In this equation, F_{in} and Δ^{33}_{in} represent the flux and sulphur isotope composition, respectively, of the summed inputs to the surface system. Isotope mass balance demands that Eq. (2) sum to zero (given no known isotopically distinct sulphur loss processes from the top of Earth's atmosphere). Given this assumption and specifying:

$$f_S = \frac{F_S}{F_C + F_S} = \frac{F_S}{F_{in}} \ , \tag{3}$$

gives:

$$\Delta^{33}_{in} = \Delta^{33}_{S}(1 - f_S) + \Delta^{33}_{C} f_S \ . \tag{4}$$

This allows us to estimate the globally averaged sulphur isotope anomaly accumulating in the weatherable crust at any given time at steady state, assuming a composite Δ^{33}_{in} value and values for Δ^{33}_{S} and f_S.

The results of this calculation are shown in Fig. S3, under the scenario that the composite input flux to the surface sums to $\Delta^{33}S = 0‰$. It is clear that a wide range of Δ_S^{33} and f_S values can conspire to elevate Δ_C^{33}. Values of Δ_S^{33} should essentially track the isotopic composition of seawater sulphate. This value, although possibly non-conservative within sulphate-deficient Archaean oceans, can be constrained by measurements of marine sulphate and sulphide minerals. In the latter case, values from sedimentary sulphides provide a maximum estimate of the $\Delta^{33}S$ value of contemporaneous sulphate – the most ^{33}S-depleted sulphides typically range between values of -1‰ and -4‰, and it is possible that contemporaneous seawater sulphate $\Delta^{33}S$ values were well below this.

Values for the parameter f_S are more difficult to constrain. Recent estimates of the rate of net sulphate reduction and sulphur burial in deep-sea sediments are on the order of ~4 – 30 x 10^{-8} molS cm^{-2} y^{-1} (ref. 48-50). When conservatively scaled to depths below ~4000m (i.e., ~50% of modern seafloor area[51]), these rates yield overall sulphur fluxes between ~7 – 50 x 10^{10} molS y^{-1}. Note that the upper end of this range is greater than estimates of the modern volcanic sulphur flux. On the one hand, it is likely that rates of sulphate reduction and sulphur burial in deep-sea sediments are quite variable (e.g., ref. 52) and that scaling single rates to extremely large regions of the seafloor will provide only a very rough estimate. More importantly, however, the magnitude of carbon flux through other terminal electron acceptors prior to sulphate reduction in modern well-ventilated oceans ensures that such an estimate will likely be conservative with respect to the pervasively reducing conditions in Archaean oceans, and should be viewed as a lower estimate for a reducing deep sea.

An alternative approach, following ref. 53, is to estimate the theoretical maximum for this parameter on the modern Earth by combining rates of sediment subduction[54-57] with the typical reactive Fe content of deep-sea sediments[58] and the assumption that most or all this reactive Fe is sequestered as a constituent of pyrite. This approach yields an estimate on the order of 4 – 9 x 10^{11} molS y^{-1}, a very large sulphur flux in the context of a surface system driven almost entirely by volcanic sulphur input (see below). It is crucial to point out that, in principle, this theoretical maximum will only quantitatively apply to an anoxic and sulfidic (euxinic) deep ocean, in which pyrite formation and burial are necessarily limited by reactive Fe. However, studies of modern sulphate-deficient analog environments suggest that significant sulphur burial fluxes can be sustained in systems with very efficient capture of dissolved sulphide, which is primarily a function of elevated reactive Fe availability[59,60]. In other words, there is no *a priori* reason to suspect that a sulphate-deficient and Fe-buffered (ferruginous) deep ocean would sequester sulphur as sedimentary pyrite any less efficiently than a euxinic deep sea. Indeed, the development of euxinia on a large scale (i.e., the accumulation of dissolved sulphide in marine water masses) necessarily implies that sulphide capture and burial are operating below peak efficiency.

A third approach to conceptualizing the burial ratio of sulphur between deep-sea and marginal environments is to consider the relative carbon fluxes characteristic of continental margin and open ocean settings. On the modern Earth, open ocean primary productivity is locally very low relative to continental margins[61-63]. However, when integrated over large areas the overall rates

of production in open ocean settings account for ~85-90% of global marine primary production[64,65] and ~70% of carbon export flux from the photic zone[65]. In the modern ocean the vast majority of this carbon is, of course, consumed through aerobic respiration in the water column. However, much or most of this carbon export flux would be consumed by microbial sulphate reduction in a reducing ocean. In addition, dissolved O_2 concentrations in the modern ocean are rarely drawn down to values approaching zero despite the fact that the vast majority of respired carbon on the modern Earth is redox-coupled to O_2. This simple observation, combined with the observation that aerobic respiration stoichiometrically consumes twice as much of its terminal electron acceptor as sulphate reduction per mol of organic matter, indicates that dissolved sulphate concentrations of ~100-200μM (ref. 66, 67) would not be readily exhausted in an open water column, allowing for extensive water column sulfide formation given the effectively limitless reactive Fe availability in ferruginous Archaean oceans. As a result, in an ocean that is pervasively reducing and Fe^{2+}-buffered we would expect that the partitioning of relative sulphur burial between continental margin and deep-sea settings will roughly track relative differences in primary and export production. In fact, marginal settings where carbon fluxes are locally much higher are much more likely to be characterized by Fe-limited pyrite formation[68,69], and sulphur burial in such settings would thus be relatively inefficient.

Although these considerations are inherently illustrative, they serve to demonstrate that the mass flux of sulphur associated with the subduction of deep-sea sediments can in principle be substantial, and could plausibly represent a large relative sulphur flux in an Earth surface sulphur cycle dominated by volcanic inputs. This flux, and its relative isotopic imprint within the weathering crust, would also be expected to vary as a function of temporally dynamic tectonic processes through the combined effects of sediment subduction and volcanic outgassing. We note, however, that sediment subduction as an important Earth surface process is likely to have been operative since very early in Earth's history[70-77]. In addition, it is clear from Eq. (4) that small inputs of solubilized sulphur from the weathering crust as a result of low-level oxidative processing (e.g., ref. 40, 68, 78-80) could potentially act to greatly amplify any isotopic asymmetry initialized as described above.

Model Setup:

Our model tracks the material transfer and isotopic composition of three Earth surface sulphur reservoirs (Main Text Figure 2): an oceanic sulphate reservoir (M_{sw}) and two crustal sulphur reservoirs [referred to, following ref. 81-85, as "young" (M_y) and "old" (M_o)]. The distinction between two crustal reservoirs of varying cycling speeds was initially introduced to more directly couple the carbon and sulphur isotope composition of fluxes out of the ocean to that of input fluxes to the ocean, in an effort to alleviate physically unrealistic shifts in atmospheric composition due to changes in measured isotope ratios of sedimentary carbonate and sulphate minerals[81,83]. However, there is also ample geological justification for such a model configuration[81-87], and subsequent work has shown that this assumption results in a good agreement between proxy-based reconstructions of Phanerozoic atmospheric composition and those derived from mass balance models[85,88-91].

The dynamics of the seawater sulphate reservoir (M_{sw}) through time are governed by the input fluxes of sulphur associated with weathering of sulphides from both of the modeled sedimentary reservoirs ($F_{w,y}$ and $F_{w,o}$), weathering of sulphide from an igneous (and thus isotopically normal) reservoir ($F_{w,ig}$), and volcanic sulphur emissions (F_v), balanced against the removal of sulphur from the ocean in association with the burial of sedimentary pyrite ($F_{b,py}$). The mass of the rapidly weathering pyrite reservoir (M_y) is similarly controlled by the balance between inputs associated with pyrite burial ($F_{b,py}$) and outputs due to both weathering at the surface ($F_{w,y}$) and gradual removal into the old sulphur reservoir[81-85] ($F_{y\text{-}o}$). The mass of the slowly weathering pyrite reservoir (M_o) is regulated by the balance between inputs from the young reservoir and outputs due to weathering. These relationships can be summarized as:

$$\frac{dM_{sw}}{dt} = F_{w,y} + F_{w,o} + F_v + F_{w,ig} - F_{b,py} \ , \tag{5}$$

$$\frac{dM_y}{dt} = F_{b,py} - F_{w,y} - F_{y-o} \ , \tag{6}$$

$$\frac{dM_o}{dt} = F_{y-o} - F_{w,o} \ . \tag{7}$$

We assume that the deep ocean is Fe^{2+}-buffered[92-96]. Conceptually, this means that hydrothermal sulphide introduced to the ocean through seawater-basalt interaction is negligible due to near vent iron sulphide precipitation, and is thus assumed not to participate in the isotope mass balance of oceanic sulphur.

Isotope mass balance equations can be similarly obtained for each reservoir:

$$\frac{d}{dt}\left(M_{sw}\delta^{3x}_{sw}\right) = F_{w,y}\delta^{3x}_{y} + F_{w,o}\delta^{3x}_{o} + F_v\delta^{3x}_{v} + F_{w,ig}\delta^{3x}_{w,ig} - F_{b,py}\delta^{3x}_{py} \ , \tag{8}$$

$$\frac{d}{dt}\left(M_y\delta^{3x}_{y}\right) = F_{b,py}\delta^{3x}_{py} - F_{w,y}\delta^{3x}_{y} - F_{y\text{-}o}\delta^{3x}_{y} \ , \tag{9}$$

$$\frac{d}{dt}\left(M_o\delta^{3x}_{o}\right) = F_{y\text{-}o}\delta^{3x}_{y} - F_{w,o}\delta^{3x}_{o} \ , \tag{10}$$

where δ values refer to the isotopic composition of each reservoir, defined according to traditional delta notation in "per mille" (‰), and x = 3, 4, or 6. All flux terms are first-order and of the form:

$$F_i = k_i M_i \ , \tag{11}$$

where the subscripts "i" refer to a given flux, and "k_i" refers to the rate constant associated with each flux parameterization. The magnitude of a given flux thus depends largely on the size of the reservoir from which the flux is derived. Two exceptions are the volcanic flux (F_v) and the igneous weathering flux ($F_{w,ig}$), which are varied between runs but imposed as constants within a given run.

The equations for material and isotope mass balance can be combined and simplified to yield equations describing how the isotopic composition of a given reservoir evolves with time as a function of the fluxes into and out of the reservoir and their isotopic composition:

$$M_{sw}\frac{d\delta_{sw}^{3.x}}{dt} = \sum_i [F_i(\delta_i^{3.x} - \delta_{sw}^{3.x})] - F_{b,py}\Delta_{py}^{3.x} \quad , \tag{12}$$

$$M_{y}\frac{d\delta_{y}^{3.x}}{dt} = F_{b,py}(\delta_{py}^{3.x} - \delta_{y}^{3.x}) \quad , \tag{13}$$

$$M_{o}\frac{d\delta_{o}^{3.x}}{dt} = F_{y-o}(\delta_{y}^{3.x} - \delta_{o}^{3.x}) \quad . \tag{14}$$

where i in Eq. 12 refers to a given component of the overall input flux to the ocean. Note that the isotopic fractionation between seawater sulphate and sedimentary pyrite ($\Delta_{py}^{3.x}$) is expressed as a negative number in the above equations. This parameter is defined, with reference to ^{34}S, using a Monod-type function:

$$\Delta_{py}^{34} = \Delta_{MAX}^{34}\frac{[SO_4^{2-}]_{sw}}{K_m^{\Delta} + [SO_4^{2-}]_{sw}} \quad , \tag{15}$$

where Δ_{MAX}^{34} refers to the maximum metabolic fractionation associated with microbial sulphate reduction (as expressed on a global scale), $[SO_4^{2-}]_{sw}$ is the ambient seawater sulphate concentration (calculated from M_{sw} assuming an ocean volume of 1.37 x 10^{21} L), and K_m^{Δ} represents a "pseudo-half-saturation" constant derived empirically from chemostat experiments with *A. fulgidus* (ref. 97). Our reference model uses Δ_{MAX}^{34} = 30‰ and K_m^{Δ} = 0.363 mM, but these values have no effect on the magnitude of the $\Delta^{33}S$ signal through time and will only influence model trajectories in $\delta^{34}S - \Delta^{33}S$ space. Microbial fractionations are related to the other isotopes assuming mass-dependence:

$$\Delta_{py}^{33} = {}^{33}\lambda\,\Delta_{py}^{34} \tag{16}$$

$$\Delta_{py}^{36} = {}^{36}\lambda\,\Delta_{py}^{34} \tag{17}$$

where $^{33}\lambda = 0.515$ and $^{36}\lambda = 1.890$ (e.g., ref. 98).

Model parameters for our reference case (Main Text Fig. 3) are shown in Table S1. Parameter values for the reference case were chosen to approximately satisfy known constraints on: (1) the overall size of the crustal sulphur reservoir[53,81,99,100]; (2) the residence time of sulphur as it cycles through the exogenic system[87,101]; (3) the fraction of overall sulphur input derived from the rapidly recycling sulphur reservoir[85,102-105]; (4) the residence time of sulphur in the rapidly recycling reservoir with respect to weathering[81,82]; and, (5) the residence time of sulphur in the rapidly recycling reservoir with respect to removal to the old reservoir[81,85,105] (the "aging flux" of the young pyrite reservoir). The range of F_v values was chosen to encompass estimates of the modern volcanic sulphur flux and values scaled up to reflect the possibility of greater crustal heat flow and volcanic activity during Earth's early history. Estimates of the modern volcanic sulphur

flux are typically on the order of ~2-3 x 10^{11} mol y^{-1} (ref. 53, 106-110), and we use an estimate of 2 x 10^{11} mol y^{-1} as our low volcanic flux. Heat flow through the crust has declined with time, and as a result it is typically assumed that Earth's early history was characterized by increased rates of volcanism. Estimates vary, but it is unlikely that crustal heat flow during the Archaean was more than ~3-4 times that of the modern Earth[111-114]. We therefore use a volcanic sulphur input of 1 x 10^{12} mol y^{-1} as our high volcanic flux. We note, however, that higher rates of heat flow through the crust need not require an increase in the mass flux from subaerial volcanic activity – much of this heat loss may have been accommodated by submarine mafic spreading centers[115], which are essentially sulphur-neutral in an anoxic and iron-buffered deep ocean. In each model run, the pyrite burial rate constant (k_{py}) is solved for to attain steady state with the prescribed volcanic sulphur flux. Oxidative weathering of sedimentary and igneous rocks is then initialized, and the model evolves freely.

The Balance Between Igneous and Sedimentary Sulphur Sources

Igneous sources of sulphur within Earth's crustal reservoir can be expected to carry an isotopically normal signal when weathered. In addition, it is possible that the relative abundance within the crust of igneous sulphur relative to sedimentary sulphur has changed throughout Earth's long history. It is thus crucial to consider whether differences in the overall balance between igneous and sedimentary sources of sulphur to the ocean relative to Phanerozoic conditions might act to dilute or significantly attenuate the crustal memory effect explored here.

On the modern Earth, igneous sulphur sources to the ocean amount to a very small fraction of the overall material balance for sulphur – approximately 3% of the input flux of sulphur to the modern ocean is derived from igneous sources[116,117]. This is despite the fact that igneous rocks cover roughly 20-30% of the weatherable area of Earth's surface[103,104,116]. The most obvious explanation for this is that igneous rocks contain, in general, much less sulphur than sedimentary rocks. This is perhaps not surprising from a mechanistic standpoint, as many igneous rocks, and in particular those which are subaerially extrusive and thus most readily incorporated into the weatherable crustal mass, lose a large fraction of their sulphur to the volatilization of sulphur-bearing gases during extrusion at the surface[118]. Rivers draining terrains dominated by igneous lithologies have far less dissolved sulphate than those draining sedimentary lithologies[116,117], consistent with the view that sedimentary rocks host the majority of the sulphur in Earth's weatherable shell.

In principle, we can estimate the possible effects of dilution by igneous sulphur with a simple two-component mixing model. This begins with the simple case of mixing two components into a single reservoir, which must satisfy mass balance:

$$[S]_{mix} = f_{ig}[S]_{ig} + (1 - f_{ig})[S]_{sed} \quad , \qquad (18)$$

where [S] refers to the sulphur content of the igneous component (*ig*), the sedimentary component (*sed*), and the resulting mixture (*mix*), and f_{ig} refers to the relative flux from the igneous component (which may vary between 0 and 1). The $\Delta^{33}S$ composition of the mixture, assuming conservative isotopic mixing, is expressed as:

$$\Delta^{33}S_{mix} = f_{ig}\Delta^{33}S_{ig}\frac{[S]_{ig}}{[S]_{mix}} + (1 - f_{ig})\Delta^{33}S_{sed}\frac{[S]_{sed}}{[S]_{mix}} \quad , \qquad (19)$$

where, in addition to the terms defined above, $\Delta^{33}S$ refers to the rare sulphur isotope compositions of the igneous flux (*ig*), the sedimentary flux (*sed*), and the resulting mixture (*mix*).

The results of such a model are shown in Fig. S4, with the normalized $\Delta^{33}S$ value of the two-component mixture plotted as a function of the relative flux from igneous sources. We set $[S]_{sed}$ at 0.6 wt% (ref. 117, 119), which is likely conservative for our purposes, and explore a range of $[S]_{ig}$ values between 10 and 1000 ppm. This range is meant to be inclusive and encompasses measurements of a wide range of extrusive, plutonic, felsic, and mafic igneous rocks[120-127]. Our preferred estimate for the overall average igneous sulphur content (300 ppm; ref. 128-130) is also shown. For comparison, the modern igneous flux component and the estimated range of fractional exposed igneous rock area on the modern Earth are also shown.

This simple exercise illustrates that it should be extremely difficult to eliminate the isotopic memory effect by invoking a larger proportion of igneous rocks in the overall weatherable rock reservoir at Earth's surface. For example, at our preferred igneous concentration a decrease in the magnitude of the $\Delta^{33}S$ anomaly in the two-component mixture by ~30% would require that well over 90% of the weathering flux must come from igneous rocks (Fig. S4). Even at the relatively high igneous sulphur concentration of 1000 ppm a similar dilution effect requires that nearly 80% of the overall weathering flux be derived by igneous rocks. We stress, however, that although these calculations are illustrative of the basic relationship they cannot capture the behavior of the full dynamic model. We therefore also explored the sensitivity of the crustal memory effect to the fractional contribution of igneous sources to the overall weathering flux (Main Text Fig. 3c), and found that even fractional contributions from the igneous weathering flux as high as 0.5 have a relatively small effect on the duration and magnitude of the isotopic residual.

There is a sound foundation supporting the notion that even a relatively large igneous component of the weatherable rock reservoir at Earth's surface will be unlikely to exert an overriding control on the isotopic composition of continentally derived sulphur. However, it is still important to ask how high we can expect the relative impact of igneous rock weathering to have been during Earth's history. The relative exposure area of igneous rocks at Earth's surface has ostensibly varied very little throughout the entire Phanerozoic[104] (the last ~500 million years of Earth's history), despite a cycle of supercontinent assembly and break-up during the late Paleozoic. In addition, recent data place the onset of significant crustal growth, recycling, emergence and surface weathering very early in Earth's history[131-138]. This is perhaps not surprising – the record of sedimentary rocks on Earth extends to ~3.8 billion years ago and is continuous from this point onward, suggesting qualitatively that a surface sedimentary rock cycle existed during Earth's earliest history. Once significant crustal exhumation begins, the formation of a sedimentary shell at Earth's surface will proceed extremely rapidly – from a geologic point of view (e.g., ref. 139).

Exploration of Sm/Nd systematics reveals that the chemical evolution of the upper crust is best explained through a steady-state sedimentary rock cycle model in which (roughly) >60% of the

sedimentary rock mass is "cannibalistic", i.e., is derived from the deposition of previously weathered sedimentary rocks[140,141]. The remainder represents the fraction of deposited sediments that become subducted, which is balanced by the formation of new sediment from the exposure and weathering of primary igneous rocks. In other words, these results imply that less than ~40% of the sedimentary rock mass at any given time is derived from the weathering of primary igneous rocks, and this value can be broadly applied coherently to most of Earth's history subsequent to the establishment of a sedimentary shell.

Perhaps even more importantly, values below or even approaching 50% (i.e., a relative igneous contribution, with respect to area, of 0.5) are inconsistent with the record of Sm/Nd systematics through time[140]. For our purposes, it is crucial to point out that a relative weatherable area of even 50% will almost certainly correspond to a much smaller relative contribution to the overall sulphur flux – again, the modern cycle is characterized by ~20-30% relative exposure of igneous rocks, but these account for only ~3% of the flux of sulphur to the ocean. Although it is difficult to pinpoint precisely the inception of a steady-state cannibalistic sedimentary rock cycle based on the current sediment Sm/Nd isotope record alone, it is likely to have been in operation for over 3 billion years, consistent with evidence for significant early Archaean crustal recycling. In short, a relative areal coverage of igneous rocks of ~0.5 would seem to be an upper limit, and this would almost certainly correspond to a much smaller relative sulphur flux as a simple consequence of much lower sulphur concentrations relative to sedimentary rocks. We therefore consider in our model a relative igneous flux value of 0.5 to be a rather extreme upper limit, and suggest that even approaching this value would be very difficult.

Table S1. Model parameters and values used in our reference model. See text for details.

Parameter	Description	Reference Model Value
M_{sw}	seawater sulphate mass	2.74 x 10^{17} mol
M_y	mass of rapidly weathering (young) pyrite reservoir	5 x 10^{19} mol
M_o	mass of slowly weathering (old) pyrite reservoir	3 x 10^{20} mol
M_{tot}	Earth surface sulphur reservoir mass	3.5 x 10^{20} mol
k_y	young pyrite weathering rate constant	2 x 10^{-8} y^{-1}
k_o	old pyrite weathering rate constant	1 x 10^{-9} y^{-1}
k_{avg}	overall crustal sulphur weathering rate constant	3.7 x 10^{-9} y^{-1}
k_{py}	pyrite burial rate constant	[solved]
τ_{weath}	residence time of rapidly weathering pyrite reservoir with respect to weathering	50 x 10^6 y
$\tau_{y\text{-}o}$	residence time of rapidly weathering pyrite reservoir with respect to conversion to old reservoir ("aging flux")	170 x 10^6 y
τ_{mean}	mean residence time of surface crustal sulphur	270 x 10^6 y
F_y / F_{tot}	fraction of overall weathering flux derived from rapidly weathering sulphur reservoir	0.77
F_v	volcanic sulphur flux	6.0 x 10^{11} mol y^{-1}
$F_{w,ig}$	igneous sulphur weathering flux (fraction of total weathering)	0.1
$\Delta^{33}S_{sw,i}$	initial $\Delta^{33}S$ value of seawater sulphate	-1.0‰
$\Delta^{33}S_{y,i}$	initial $\Delta^{33}S$ value of the young pyrite reservoir	3.0‰
$\Delta^{33}S_{o,i}$	initial $\Delta^{33}S$ value of the old pyrite reservoir	0.0‰
$^{33}\lambda$	mass-dependent fractionation exponent for ^{33}S	0.515
$^{36}\lambda$	mass-dependent fractionation exponent for ^{36}S	1.890
Δ^{34}_{MAX}	maximum global-scale metabolic fractionation during sulphate reduction	30‰
K^{Δ}_{m}	pseudo half-saturation constant of fractionation during sulphate reduction	0.363 mM

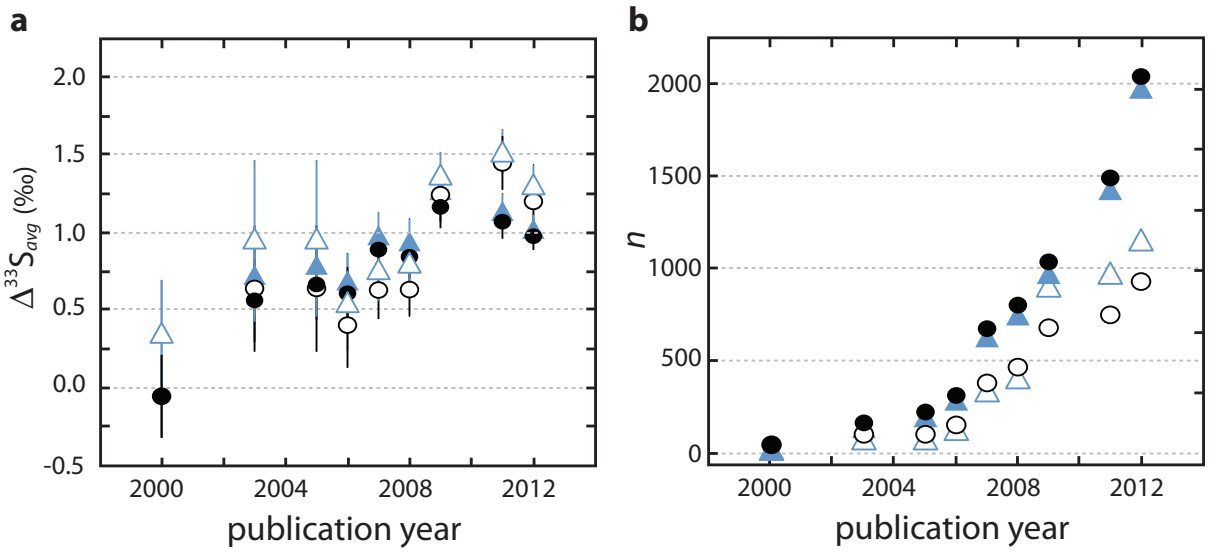

Figure S1. Cumulative average $\Delta^{33}S$ value (**a**) and database size (**b**) as a function of publication year. Filled symbols show the entire database with (circles) and without (triangles) the inclusion of sulphate minerals. Open symbols show the filtered database, with data obtained through secondary ion mass spectrometry (SIMS) analyses and data from macroscopic (often secondary) sulphide textures removed. Open symbols show the filtered database with (circles) and without (triangles) the inclusion of sulphate minerals.

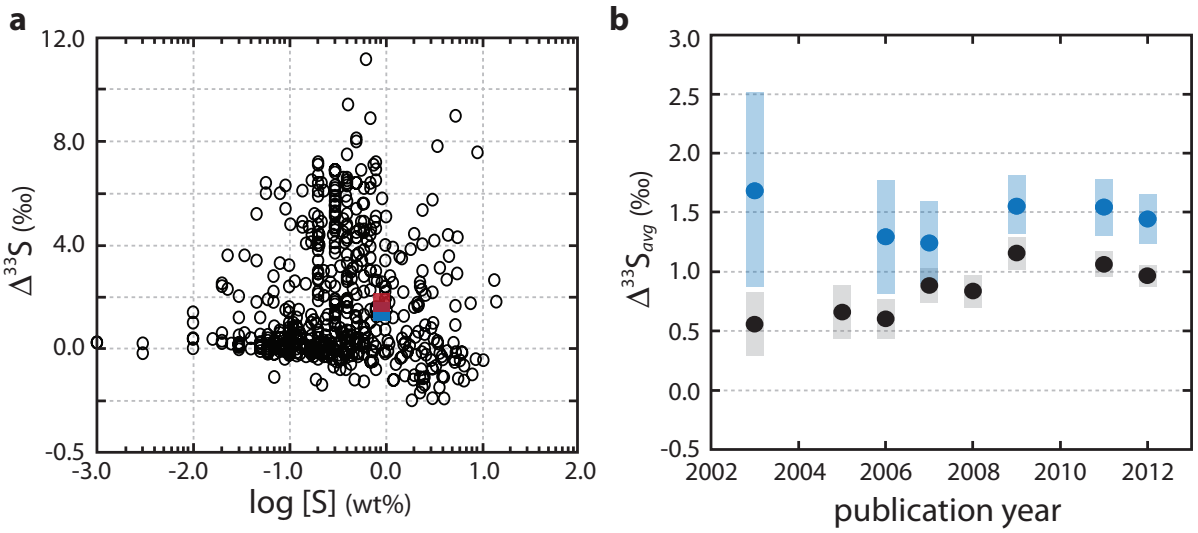

Figure S2. Bivariate plot of rare sulphur isotope composition ($\Delta^{33}S$) and sulphur concentration ([S]) (**a**), and unweighted/weighted mean $\Delta^{33}S$ values of the database as a function of database age (**b**). Note the log scale on the *x*-axis in (**a**). Open circles represent individual samples (n = 550), while the colored squares represent the overall mean value (red) and concentration-weighted mean value (blue). In (**b**), filled black circles represent unweighted mean values, while filled blue circles represent concentration-weighted mean values. The shaded boxes in (**b**) represent the 95% confidence interval about the mean.

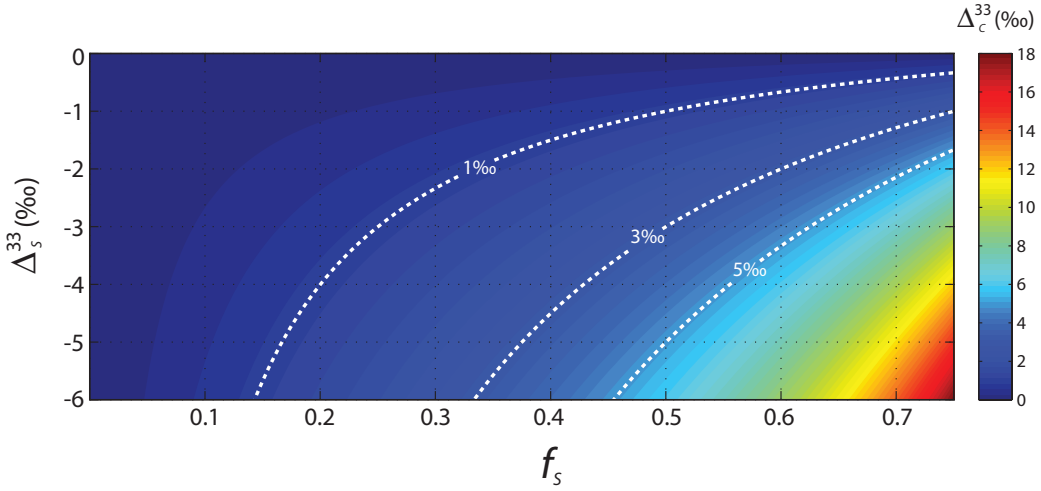

Figure S3. Results of the basic mass balance calculations for Earth surface sulphur discussed in the text. The rare sulphur isotope composition of the weathering crust (Δ^{33}_{C}) is contoured as a function of the overall fraction of sulphur exiting the surface system through subduction of marine sediments (f_S) and the rare sulphur isotope composition of the subducted sulphur pool (Δ^{33}_{S}). Note that these calculations assume a composite input value (Δ^{33}_{in}) of 0‰ and that once any isotopic asymmetry in the weathering crust is established low-level oxidative mobilization of crustal sulphides will shift all isotope contours to the left.

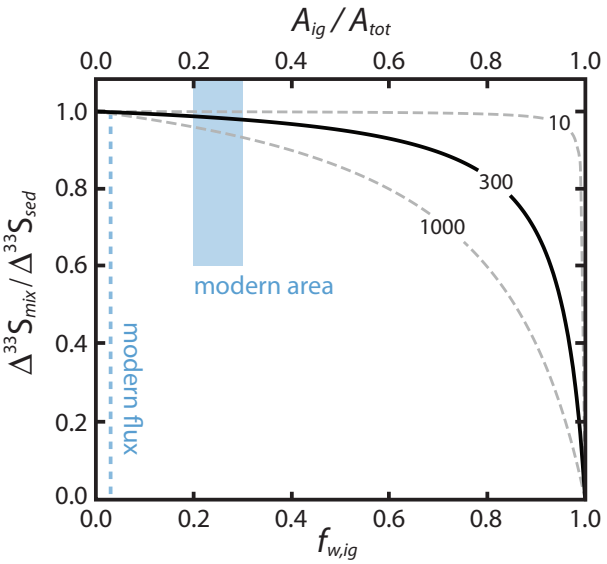

Figure S4. Results of the two-component mixing model discussed in the text, plotted with the $\Delta^{33}S$ value of the overall mixture relative to the initial sedimentary component ($\Delta^{33}S_{mix}$ / $\Delta^{33}S_{sed}$) as a function of the relative igneous sulphur flux into the system ($f_{w,ig}$). Curves are labeled by the assumed igneous sulphur concentration in ppm – the values displayed are meant to encompass a wide range of igneous rock types. Our preferred average value of 300 ppm is displayed by the solid black curve. The vertical dashed line shows the modern relative igneous flux. Also shown for comparison is the approximate relative fraction of the modern Earth's weatherable surface that is represented by igneous rocks (A_{ig}/A_{tot}; shaded box). We stress that the mixing trajectories are purely a function of the relative sulphur flux, not the relative area, but we depict the area to highlight the fact that although igneous rocks cover a relatively large portion of the modern Earth's weatherable surface they make an extremely small contribution to the overall sulphur flux.

References:

1. Farquhar, J., Bao, H., Thiemens, M. Atmospheric influence of Earth's earliest sulfur cycle. *Science* **289**, 756-758 (2000).
2. Farquhar, J. *et al.* Mass-independent sulfur of inclusions in diamond and sulfur recycling on early Earth. *Science* **298**, 2369-2372 (2002).
3. Hu, G., Rumble, D., Wang, P.-L. An ultraviolet laser microprobe for the in situ analysis of multisulfur isotopes and its use in measuring Archean sulfur isotope mass-independent anomalies. *Geochim. Cosmochim. Acta* **67**, 3101-3117 (2003).
4. Mojzsis, S.J., Coath, C.D., Greenwood, J.P., McKeegan, K.D., Harrison, T.M. Mass-independent isotope effects in Archean (2.5 to 3.8 Ga) sedimentary sulphides determined by ion microprobe analysis. *Geochim. Cosmochim. Acta* **67**, 1635-1658 (2003).
5. Ono, S. *et al.* New insights into Archean sulfur cycle from mass-independent sulfur isotope records from the Hamersley Basin, Australia. *Geochim. Cosmochim. Acta* **213**, 15-30 (2003).
6. Bekker, A. *et al.* Dating the rise of atmospheric oxygen. *Nature* **427**, 117-120 (2004).
7. Johnston, D.T. *et al.* Active microbial sulfur disproportionation in the Mesoproterozoic. *Science* **310**, 1477-1479 (2005).
8. Papineau, D., Mojzsis, S.J., Coath, C.D., Karhu, J.S., McKeegan, K.D. Multiple sulfur isotopes of sulphides from sediments in the aftermath of Paleoproterozoic glaciations. *Geochim. Cosmochim. Acta* **69**, 5033-5060 (2005).
9. Whitehouse, M.J., Kamber, B.S., Fedo, C.M., Lepland, A. Integrated Pb- and S-isotope investigation of sulphide minerals from the early Archaean of southwest Greenland. *Chem. Geol.* **222**, 112-131 (2005).
10. Cates, N.L., Mojzsis, S.J. Chemical and isotope evidence for widespread Eoarchean metasedimentary enclaves in southern West Greenland. *Geochim. Cosmochim. Acta* **70**, 4229-4257 (2006).
11. Johnston, D.T. *et al.* Evolution of the oceanic sulfur cycle at the end of the Paleoproterozoic. *Geochim. Cosmochim. Acta* **70**, 5723-5739 (2006).
12. Ohmoto, H., Watanabe, Y., Ikemi, H., Poulson, S.R., Taylor, B.E. Sulphur isotope evidence for an oxic Archaean atmosphere. *Nature* **442**, 908-911 (2006).
13. Ono, S., Wing, B., Johnston, D., Farquhar, J., Rumble, D. Mass-dependent fractionation of quadruple stable sulfur isotope system as a new tracer of sulfur biogeochemical cycles. *Geochim. Cosmochim. Acta* **70**, 2238-2252 (2006).
14. Ono, S., Wing, B., Rumble, D., Farquhar, J. High precision analysis of all four stable isotopes of sulfur (^{32}S, ^{33}S, ^{34}S and ^{36}S) at nanomole levels using a laser flourination isotope-ratio-monitoring gas chromatography-mass spectrometry. *Chem. Geol.* **225**, 30-39 (2006).
15. Bao, H., Rumble III, D., Lowe, D.R. The five stable isotope compositions of Fig Tree barites: Implications on sulfur cycle in ca. 3.2 Ga oceans. *Geochim. Cosmochim. Acta* **71**, 4868-4879 (2007).
16. Farquhar, J. *et al.* Isotopic evidence for Mesoarchaean anoxia and changing atmospheric sulphur chemistry. *Nature* **449**, 706-709 (2007).

17. Hou, K.J., Li, Y.H., Wan, D.F. Constraints on the Archean atmospheric oxygen and sulfur cycle from mass-independent sulfur records from Anshan-Benxi BIFs, Liaoning Province, China. *Sci. China Ser. D – Earth Sci.* **50**, 1471-1478 (2007).
18. Kaufman, A.J. *et al.* Late Archean biospheric oxygenation and atmospheric evolution. *Science* **317**, 1900-1903 (2007).
19. Kamber, B.S., Whitehouse, M.J. Micro-scale sulphur isotope evidence for sulphur cycling in the late Archean shallow ocean. *Geobiology* **5**, 5-17 (2007).
20. Ono, S., Shanks III, W.C., Rouxel, O.J., Rumble, D. S-33 constraints on the seawater sulphate contribution in modern seafloor hydrothermal vent sulphides. *Geochim. Cosmochim. Acta* **71**, 1170-1182 (2007).
21. Papineau, D., Mojzsis, S.J., Schmitt, A.K. Multiple sulfur isotopes from Paleoproterozoic Huronian interglacial sediments and the rise of atmospheric oxygen. *Earth Planet. Sci. Lett.* **255**, 188-212 (2007).
22. Philippot, P. *et al.* Early Archaean microorganisms preferred elemental sulfur, not sulphate. *Science* **317**, 1534-1537 (2007).
23. Domagal-Goldman, S.D., Kasting, J.F., Johnston, D.T., Farquhar, J. Organic haze, glaciations and multiple sulfur isotopes in the Mid-Archean Era. *Earth Planet. Sci. Lett.* **269**, 29-40 (2008).
24. Johnston, D.T. *et al.* Sulfur isotope biogeochemistry of the Proterozoic McArthur Basin. *Geochim. Cosmochim. Acta* **72**, 4278-4290 (2008).
25. Johnston, D.T., Farquhar, J., Habicht, K.S., Canfield, D.E. Sulphur isotopes and the search for life: strategies for identifying sulphur metabolisms in the rock record and beyond. *Geobiology* **6**, 425-435 (2008).
26. Partridge, M.A., Golding, S.D., Baublys, K.A., Young, E. Pyrite paragenesis and multiple sulfur isotope distribution in late Archean and early Paleoproterozoic Hamersley Basin sediments. *Earth Planet. Sci. Lett.* **272**, 41-49 (2008).
27. Ueno, Y., Ono, S., Rumble, D., Maruyama, S. Quadruple sulfur isotope analysis of ca. 3.5 Ga Dresser Foromation: New evidence for microbial sulfate reduction in the early Archean. *Geochim. Cosmochim. Acta* **72**, 5675-5691 (2008).
28. Guo, Q. *et al.* Reconstructing Earth's surface oxidation across the Archean-Proterozoic transition. *Geology* **37**, 399-402 (2009).
29. Ono, S., Beukes, N.J., Rumble, D. Origin of two distinct multiple-sulfur isotope compositions of pyrite in the 2.5 Ga Klein Naute Formation, Griqualand West Basin, South Africa. *Precambrian Res.* **169**, 48-57 (2009).
31. Ono, S., Kaufman, A.J., Farquhar, J., Sumner, D.Y., Beukes, N.J. Lithofacies control on multiple-sulfur isotope records and Neoarchean sulfur cycles. *Precambrian Res.* **169**, 58-67 (2009).
31. Shen, Y., Farquhar, J., Masterson, A., Kaufman, A.J., Buick, R. Evaluating the role of microbial sulphate reduction in the early Archean using quadruple isotope systematics. *Earth Planet. Sci. Lett.* **279**, 383-391 (2009).
32. Thomazo, C., Ader, M., Farquhar, J., Philippot, P. Methanotrophs regulated atmospheric sulfur isotope anomalies during the Mesoarchean (Tumbiana Formation, Western Australia). *Earth Planet. Sci. Lett.* **279**, 65-75 (2009).
33. Wu, N., Farquhar, J., Strauss, H., Kim, S.-T., Canfield, D.E. Evaluating the S-isotope fractionation associated with Phanerozoic pyrite burial. *Geochim. Cosmochim. Acta* **74**, 2053-2071 (2010).

34. Williford, K.H., Van Kranendonk, M.J., Ushikubo, T., Kozdon, R., Valley, J.W. Constraining atmospheric oxygen and seawater sulfate concentrations during Paleoproterozoic glaciation: In situ sulfur three-isotope microanalysis of pyrite from the Turee Creek Group, Western Australia. *Geochim. Cosmochim. Acta* **75**, 5686-5705 (2011).
35. Zerkle, A.L., Claire, M.W., Domagal-Goldman, S.D., Farquhar, J., Poulton, S.W. A bistable organic-rich atmosphere on the Neoarchaean Earth. *Nat. Geosci.* **5**, 359-363 (2012).
36. Guy, B.M. *et al.* A multiple sulfur and organic carbon isotope record from non-conglomeratic sedimentary rocks of the Mesoarchean Witwatersrand Supergroup, South Africa. *Precambrian Res.* **216-219**, 208-231 (2012).
37. Philippot, P., van Zuilen, M., Rollion-Bard, C. Variations in atmospheric sulphur chemistry on early Earth linked to volcanic activity. *Nat. Geosci.* **5**, 668-674 (2012).
38. Nelson, D.R., Trendall, A.F., Altermann, W. Chronological correlations between the Pilbara and Kaapvaal cratons. *Precambrian Res.* **97**, 165-189 (1999).
39. Rasmussen, B., Blake, T.S., Fletcher, I.R. U-Pb zircon age constraints on the Hamersley spherule beds: Evidence for a single 2.63 Ga Jeerinah-Carawine impact ejecta layer. *Geology* **33**, 725-728 (2005).
40. Anbar, A.D. *et al.* A whiff of oxygen before the Great Oxidation Event? *Science* **317**, 1903-1906 (2007).
41. Knoll, A.H., Beukes, N.J. Introduction: Initial investigations of a Neoarchean shelf margin-basin transition (Transvaal Supergroup, South Africa). *Precambrian Res.* **169**, 1-14 (2009).
42. Farquhar, J., Wing, B.A. Multiple sulfur isotopes and the evolution of the atmosphere. *Earth Planet. Sci. Lett.* **213**, 1-13 (2003).
43. Jamieson, J.W., Wing, B.A., Hannington, M.D., Farquhar, J. Evaluating isotopic equilibrium among sulfide mineral pairs in Archean ore deposits: Case study from the Kidd Creek VMS deposit, Ontario, Canada. *Econ. Geol.* **101**, 1055-1061 (2006).
44. Bekker, A. *et al*. Atmospheric sulfur in Archean komatiite-hosted nickel deposits. *Science* **326**, 1086-1089 (2009).
45. Brimblecombe, P. The Global Sulfur Cycle. *In* Holland, H.D., Turekian, K.K. (*eds*), *Treatise on Geochemistry* **7**, 645-682 (2003).
46. Heard, I.P.C. *et al.* A comparison of atmospheric dispersion model predictions with observations of SO_2 and sulphate aerosol from volcanic eruptions. *J. Geophys. Res.* **117**, doi:10.1029/2011JD016791 (2012).
47. Kamyshny Jr., A. Solubility of cyclooctasulfur in pure water and sea water at different temperatures. *Geochim. et Cosmochim. Acta* **73**, 6022-6028 (2009).
48. D'Hondt, S., Rutherford, S., Spivack, A.J. Metabolic activity of subsurface life in deep-sea sediments. *Science* **295**, 2067-2070 (2002).
49. D'Hondt, S. *et al.* Distributions of microbial activities in deep subseafloor sediments. *Science* **306**, 2216-2221 (2004).
50. Smith, D.C., D'Hondt, S. Exploration of life in deep subseafloor sediments. *Oceanography* **19**, 58-70 (2006).
51. Menard, H.W., Smith, S.M. Hypsometry of ocean basin provinces. *J. Geophys. Res.* **71**, 4305-4325 (1966).

52. Canfield, D.E. Sulfate reduction in deep-sea sediments. *Am. J. Sci.* **291**, 177-188 (1991).
53. Canfield, D.E. The evolution of the Earth surface sulfur reservoir. *Am. J. Sci.* **304**, 839-861 (2004).
54. Hay, W.M., Sloan II, J.L., Wold, C.N. Mass/age distribution and composition of sediments on the ocean floor and the global rate of sediment subduction. *J. Geophys. Res.* **93**, 14933-14940 (1988).
55. von Huene, R., Scholl, D.W. Observations at convergent margins concerning sediment subduction, subduction erosion, and the growth of continental crust. *Rev. Geophys.* **29**, 279-316 (1991).
56. Plank, T., Langmuir, C.H. The chemical composition of subducting sediment and its consequences for the crust and mantle. *Chem. Geol.* **145**, 325-394 (1998).
57. Horleston, A.C., Helffrich, G.R. Constraining sediment subduction: A converted phase study of the Aleutians and Marianas. *Earth Planet. Sci. Lett.* **359-360**, 141-151 (2012).
58. Raiswell, R., Canfield, D.E. Sources of iron for pyrite formation in marine sediments. *Am. J. Sci.* **298**, 219-245 (1998).
59. Voillier, E., Michard, G., Jézéquel, D., Pépe, M., Sarazin, G. Geochemical study of a crater lake: Lake Pavin, Puy de Dôme, France. Constraints afforded by the particulate matter distribution in the element cycling within the lake. *Chem. Geol.* **142**, 225-241 (1997).
60. Poulson Brucker, R., McManus, J., Severmann, S., Owens, J., Lyons, T.W. Trace metal enrichments in Lake Tanganyika sediments: Controls on trace metal burial in lacustrine systems. *Geochim. Cosmochim. Acta* **75**, 483-499 (2011).
61. Field, C.B., Behrenfeld, M.J., Randerson, J.T., Falkowski, P. Primary production of the biosphere: Integrating terrestrial and oceanic components. *Science* **281**, 237-240 (1998).
62. Gregg, W.W., Conkright, M.E., Ginoux, P., O'Reilly, J.E., Casey, N.W. Ocean primary production and climate: Global decadal changes. *Geophys. Res. Lett.* **30**, doi:10.1029/2003GL016889 (2003).
63. Behrenfeld, M.J. *et al.* Climate-driven trends in contemporary ocean productivity. *Nature* **444**, 752-755 (2006).
64. Muller-Karger, F.E. *et al.* The importance of continental margins in the global carbon cycle. *Geophys. Res. Lett.* **32**, doi:10.1029/2004GL021346 (2005).
65. Dunne, J.P., Sarmiento, J.L., Gnanadesikan, A. A synthesis of global particle export from the surface ocean and cycling through the ocean interior and on the seafloor. *Global Biogeochem. Cyc.* **21**, doi:10.1029/2006GB002907 (2007).
66. Habicht, K.S., Gade, M., Thamdrup, B., Berg, P., Canfield, D.E. (2002) Calibration of sulfate levels in the Archean ocean. *Science* **298**, 2372-2374 (2002).
67. Halevy, I., Johnston, D.T., Schrag, D.P. Explaining the structure of the Archean mass-independent sulfur isotope record. *Science* **329**, 204-207 (2010).
68. Reinhard, C.T., Raiswell, R., Scott, C., Anbar, A.D., Lyons T.W. A late Archean sulfidic sea stimulated by early oxidative weathering of the continents. *Science* **326**, 713-716 (2009).
69. Poulton, S.W., Fralick, P.W., Canfield, D.E. Spatial variability in oceanic redox structure 1.8 billion years ago. *Nat. Geosci.* **3**, 486-490 (2010).

70. Sleep, N.H. Evolution of the continental lithosphere. *Ann. Rev. Earth Planet. Sci.* **33**, 369-393 (2005).
71. Cawood, P.A., Kröner, A., Pisarevsky, S. Precambrian plate tectonics: Criteria and evidence. *GSA Today* **16**, 4-11 (2006).
72. Condie, K.C., Kröner, A. When did plate tectonics begin? Evidence from the geologic record. *GSA Spec. Pap.* **440**, 281-294 (2008).
73. Hopkins, M., Harrison, T.M., Manning, C.E. Low heat flow inferred from >4 Gyr zircons suggests Hadean plate boundary interactions. *Nature* **456**, 493-496 (2008).
74. Hopkins, M.D., Harrison, T.M., Manning, C.E. Constraints on Hadean geodynamics from mineral inclusions in >4 Ga zircons. *Earth Planet. Sci. Lett.* **298**, 367-376 (2010).
75. Van Kranendonk, M.J., Smithies, R.H., Hickman, A.H., Wingate, M.T.D., Bodorkos, S. Evidence for Mesoarchean (~3.2 Ga) rifting of the Pilbara Craton: The missing link in an early Precambrian Wilson cycle. *Precam. Res.* **177**, 145-161 (2010).
76. Ganne, J. *et al.* Modern-style plate subduction preserved in the Palaeoproterozoic West African craton. *Nat. Geosci.* **5**, 60-65 (2012).
77. Fowler, M., Robinson, H. Phanerozoic sanukitoids from Caledonian Scotland: Implications for Archean subduction. *Geology* **40**, 1079-1082 (2012).
78. Kasting, J.F., Holland, H.D., Pinto, J.P. Oxidant abundances in rainwater and the evolution of atmospheric oxygen. *J. Geophys. Res.* **90**, 10497-10510 (1985).
79. Williamson, M.A., Rimstidt, J.D. The kinetics and electrochemical rate-determining step of aqueous pyrite oxidation. *Geochim. Cosmochim. Acta* **58**, 5443-5454 (1994).
80. Stüeken, E.E., Catling, D.C., Buick, R. Contributions to late Archaean sulphur cycling by life on land. *Nat. Geosci.* **5**, 722-725 (2012).
81. Berner, R. Models for carbon and sulfur cycles and atmospheric oxygen: Application to Paleozoic geologic history. *Am. J. Sci.* **287**, 177-196 (1987).
82. Berner, R.A., Canfield, D.E. A new model for atmospheric oxygen over Phanerozoic time. *Am. J. Sci.* **289**, 333-361 (1989).
83. Berner, R.A. Biogeochemical cycles of carbon and sulfur and their effect on atmospheric oxygen over Phanerozoic time. *Palaeogeogr. Palaeoclim. Palaeoecol.* **75**, 97-122 (1989).
84. Berner, R.A. Modeling atmospheric O_2 over Phanerozoic time. *Geochim. Cosmochim. Acta* **65**, 685-694 (2001).
85. Berner, R.A. GEOCARBSULF: A combined model for Phanerozoic atmospheric O_2 and CO_2. *Geochim. Cosmochim. Acta* **70**, 5653-5664 (2006).
86. Garrels, R.M., Mackenzie, F.T. Sedimentary rock types: Relative proportions as a function of geological time. *Science* **163**, 570-571 (1969).
87. Garrels R.M., Mackenzie, F.T. A quantitative model for the sedimentary rock cycle. *Mar. Chem.* **1**, 27-41 (1972).
88. Royer, D.L., Berner, R.A., Beerling D.J. Phanerozoic atmospheric CO_2 change: evaluating geochemical and paleobiological approaches. *Earth Sci. Rev.* **54**, 349-392.
89. Royer D.L., Berner, R.A., Park, J. Climate sensitivity constrained by CO_2 concentrations over the past 420 million years. *Nature* **446**, 530-532 (2007).
90. Berner R.A., Kothavala, Z. GEOCARB III: A revised model of atmospheric CO_2 over Phanerozoic time. *Am. J. Sci.* **301**, 182-204 (2001).

91. Scott A.C., Glasspool I.J. The diversification of Paleozoic fire systems and fluctuations in atmospheric oxygen concentration. *Proc. Nat. Acad. Sci. USA* **103**, 10861-10865 (2001).
92. Holland, H.D. The oceans: A possible source of iron in iron-formations. *Econ. Geol.* **68**, 1169-1172 (1973).
93. Holland, H.D. *The Chemical Evolution of the Atmosphere and Oceans*. Princeton, NJ, Princeton University Press, 582pp (1984)
94. Sumner, D.Y. Carbonate precipitation and oxygen stratification in late Archean seawater as deduced from facies and stratigraphy of the Gamohaan and Frisco formations, Transvaal Supergroup, South Africa. *Am. J. Sci.* **297**, 455-487 (1997).
95. Canfield, D.E. The early history of atmospheric oxygen: Homage to Robert M. Garrels. *Ann. Rev. Earth Planet. Sci.* **33**, 1-36 (2005).
96. Kump, L.R., Seyfried Jr., W.E. Hydrothermal Fe fluxes during the Precambrian: Effect of low oceanic sulphate concentrations and low hydrostatic pressure on the composition of black smokers. *Earth Planet. Sci. Lett.* **235**, 654-662 (2005).
97. Habicht, K.S., Salling, L., Thamdrup, B., Canfield, D.E. Effect of low sulphate concentrations on lactate oxidation and isotope fractionation during sulphate reduction by *Archaeoglobus fulgidus* Strain Z. *App. Env. Microbiol.* **71**, 3770-3777 (2005).
98. Farquhar, J. *et al.* Multiple sulphur isotopic interpretations of biosynthetic pathways: implications for biological signatures in the sulphur isotope record. *Geobiology* **1**, 27-36.
99. Li, Y.-H. Geochemical mass balance among lithosophere, hydrosphere, and atmosphere. *Am. J. Sci.* **272**, 119-137 (1972).
100. Garrels R.M., Lerman, A. Coupling of the sedimentary sulfur and carbon cycles – An improved model. *Am. J. Sci.* **284**, 989-1007 (1984).
101. Kump, L.R., Garrels, R.M. Modeling atmospheric O_2 in the global sedimentary redox cycle. *Am. J. Sci.* **286**, 337-360 (1986).
102. Garrels, R.M., Lerman, A., Mackenzie, F.T. Controls of atmospheric O_2 and CO_2: Past, present, and future. *Am. Sci.* **64**, 306-315 (1976).
103. Blatt, H., Jones, R.L. Proportions of exposed igneous, metamorphic, and sedimentary rocks. *GSA Bull.* **86**, 1085-1088 (1975).
104. Bluth, G.J.S., Kump, L.R. Phanerozoic paleogeology. *Am. J. Sci.* **291**, 284-308 (1991).
105. Berner, R.A. A model for atmospheric CO_2 over Phanerozoic time. *Am. J. Sci.* **291**, 339-376 (1991).
106. Berresheim, H., Jaeschke, W. The contribution of volcanoes to the global atmospheric sulfur budget. *J. Geophys. Res.* **88**, 3732-3740 (1983).
107. Walker, J.C.G., Brimblecombe, P. Iron and sulfur in the pre-biologic ocean. *Precambrian Res.* **28**, 205-222 (1985).
108. Andres, R.J., Kasgnoc, A.D. A time-averaged inventory of subaerial volcanic sulfur emissions. *J. Geophys. Res.* **103**, 25251-25261 (1998).
109. Halmer, M.M., Schmincke, H.-U., Graf, H.-F. The annual volcanic gas input into the atmosphere, in particular to the stratosphere: a global data set for the past 100 years. *Jour. Volcanol. Geotherm. Res.* **115**, 511-528 (2002).

110. Canfield, D.E., Rosing, M.T., Bjerrum, C. Early anaerobic metabolisms. *Phil. Trans. R. Soc. B* **361**, 1819-1836 (2006).
111. Schubert, G., Stevenson, D., Cassen, P. Whole planet cooling and the radiogenic heat source contents of the Earth and Moon. *J. Geophys. Res.* **85**, 2531-2538 (1980).
112. Christensen, U.R. Thermal evolution models for the Earth. *J. Geophys. Res.* **90**, 2995-3007 (1985).
113. Lenardie, A. Continental growth and the Archean paradox. *Geophys. Monog. Ser.* **164**, 33-45 (2006).
114. Padhi, C.M., Korenaga, J., Ozima, M. Thermal evolution of Earth with xenon degassing: A self-consistent approach. *Earth Planet. Sci. Lett.* **341-344**, 1-9 (2012).
115. Kump, L.R., Barley, M.E. Increased subaerial volcanism and the rise of atmospheric oxygen 2.5 billion years ago. *Nature* **448**, 1033-1036 (2007).
116. Meybeck, M. Global chemical weathering of surficial rocks estimated from river dissolved loads. *Am. J. Sci.* **287**, 401-428 (1987).
117. Berner, E.K., Berner, R.A. *Global Environment: Air, Water, and Geochemical Cycles.* Prentice-Hall, Upper Saddle River, NJ (1996).
118. Moore, J.G., Fabbi, B.P. An estimate of the juvenile sulfur content of basalt. *Contr. Mineral. and Petrol.* **33**, 118-127 (1971).
119. Holland, H.D. *The Chemistry of the Atmosphere and Oceans*. Wiley, New York, NY (1978).
120. Naldrett, A.J., Goodwin, A.M., Fisher, T.L., Ridler, R.H. The sulfur content of Archean volcanic rocks and a comparison with ocean floor basalts. *Can. J. Earth. Sci.* **15**, 715-728 (1978).
121. Sakai, H., Ueda, A. Sulfur and carbon isotope ratios of dacite and rhyolite conglomerates from Site 439, Leg 57, Deep Sea Drilling Project. *In* Lee, M., Stout, L.N. (*eds*), *Proc. ODP, Sci. Results* **57**, 1285-1288 (1980).
122. Ueda, A., Sakai, H. Simultaneous determinations of the concentration and isotope ratio of sulfate- and sulfide-sulfur and carbonate-carbon in geological samples. *Geochemical Journal* **17**, 185-196 (1983).
123. Ishihara, S., Sasaki, A. Sulfur isotopic ratios of the magnetite-series and ilmenite-series granitoids of the Sierra Nevada batholith – A reconnaissance study. *Geology* **17**, 788-791 (1989).
124. Torssander, P. Sulfur isotope ratios of Leg 126 igneous rocks. *In* Taylor, B., Fujioka, K., et al., *Proc. ODP, Sci. Results* **126**, 449-453 (1992).
125. Alt, J.C., Shanks III, W.C., Jackson, M.C. Cycling of sulfur in subduction zones: The geochemistry of sulfur in the Mariana Island Arc and back-arc trough. *Earth Planet. Sci. Lett.* **119**, 477-494 (1993).
126. Puchelt, H., Prichard, H.M., Berner, Z., Maynard, J. Sulfide mineralogy, sulfur content, and sulfur isotope composition of mafic and ultramafic rocks from Leg 147. *In* Mével, C., Gillis, K.M., Allan, J.F., Meyer, P.S. (*eds*), *Proc. ODP, Sci. Results* **147**, 91-101 (1996).
127. Hong, Y-D., Namgung, S-W., Yoshida, M., Malik, A. Determination of ultra-micro amounts of sulfur in igneous rocks by spectroflourimetry using 2-(o-hydroxyphenyl) benzoxazole derivatization and tin(II)-strong phosphoric acid-assisted reduction. *Talanta* **51**, 291-301 (2000).

128. Turekian, K.K., Wedepohl, K.H. Distribution of the elements in some major units of the Earth's crust. *GSA Bulletin* **72**, 175-192 (1961).
129. Taylor, S.R. Abundance of chemical elements in the continental crust: a new table. *Geochim. Cosmochim. Acta* **28**, 1273-1285 (1964).
130. McDonough, W.F., Sun, S.-s. The composition of the Earth. *Chem. Geol.* **120**, 223-253 (1995).
131. Wronkiewicz, D.J., Condie, K.C. Geochemistry and provenance of sediments from the Pongola Supergroup, South Africa: Evidence for a 3.0-Ga-old continental craton. *Geochim. Cosmochim. Acta* **53**, 1537-1549 (1989).
132. Green, M.G., Sylvester, P.J., Buick, R. Growth and recycling of early Archaean continental crust: geochemical evidence from the Coonterunah and Warrawoona Groups, Pilbara Craton, Australia. *Tectonophys.* **322**, 69-88 (2000).
133. Watson, E.B., Harrison, T.M. Zircon thermometer reveals minimum melting conditions on earliest Earth. *Science* **308**, 841-844 (2005).
134. Van Kranendonk, M.J., Smithies, R.H., Hickman, A.H., Champion, D.C. Review: secular tectonic evolution of Archean continental crust: interplay between horizontal and vertical processes in the formation of the Pilbara Craton, Australia. *Terra Nova* **19**, 1-38 (2007).
135. Ushikubo, T. *et al.* Lithium in Jack Hills zircons: Evidence for extensive weathering of Earth's earliest crust. *Earth Planet. Sci. Lett.* **272**, 666-676 (2008).
136. Alexander, B.W., Bau, M., Andersson, P., Dulski, P. Continentally-derived solutes in shallow Archean seawater: Rare earth element and Nd isotope evidence in iron formation from the 2.9 Ga Pongola Supergroup, South Africa. *Geochim. Cosmochim. Acta* **72**, 378-394 (2008).
137. Belousova, E.A. *et al.* The growth of the continental crust: Constraints from zircon Hf-isotope data. *Lithos* **119**, 457-466 (2010).
138. Dhuime, B., Hawkesworth, C.J., Cawood, P.A., Storey, C.D. A change in the geodynamics of continental growth 3 billion years ago. *Science* **335**, 1334-1336 (2012)
139. Veizer, J., Jansen, S.L. Basement and sedimentary recycling and continental evolution. *Journal of Geology* **87**, 341-370 (1979).
140. Veizer, J., Jansen, S.L. Basement and sedimentary recycling – 2: Time dimension to global tectonics. *Journal of Geology* **93**, 625-643 (1985).
141. Veizer, J., Mackenzie, F.T. Evolution of Sedimentary Rocks. *In* Holland, H.D., Turekian, K.K. (*eds*), *Treatise on Geochemistry* **7**, 369-407 (2003).